Subtle Changes in Clonal Dynamics Underlie the Age-Related Decline in Neurogenesis

Lisa Bast[1,2,*], Filippo Calzolari[3,4,5,*,†], Michael Strasser[1,6], Jan Hasenauer[1,2], Fabian Theis[1,2], Jovica Ninkovic[3,4,†] and Carsten Marr[1,†]

[1]Institute of Computational Biology, Helmholtz Zentrum München–German Research Center for Environmental Health, Neuherberg, Germany.
[2]Department of Mathematics, Chair of Mathematical Modeling of Biological Systems, Technische Universität München, Garching, Germany.
[3]Institute of Stem Cell Research, Helmholtz Zentrum München–German Research Center for Environmental Health, Neuherberg, Germany.
[4] Department of Physiological Genomics, Ludwig-Maximilian University, Munich, Germany.
[5]Institute for Physiological Chemistry, University Medical Center of the Johannes Gutenberg University Mainz, Mainz, Germany.
[6]Current address: Institute for Systems Biology, Seattle, WA, USA.
* These authors contributed equally
† Correspondence fcalzola@uni-mainz.de (F.C.), ninkovic@helmholtz-muenchen.de (J.N.), carsten.marr@helmholtz-muenchen.de (C.M.).

SUMMARY

Neural stem cells in the adult murine brain have only a limited capacity to self-renew, and the number of neurons they generate drastically declines with age. How cellular dynamics sustain neurogenesis and how alterations with age may result in this decline, are both unresolved issues. Therefore, we clonally traced neural stem cell lineages using confetti reporters in young and old adult mice. To understand underlying mechanisms, we derived mathematical population models of adult neurogenesis that explain the observed clonal cell type abundances. Models fitting the data best consistently show self renewal of transit amplifying progenitors and rapid neuroblast cell cycle exit. Most importantly, we identified an increase of asymmetric stem cell divisions at the expense of symmetric stem cell differentiation with age. Beyond explaining existing longitudinal population data, our model identifies a particular cellular strategy underlying adult neural stem cell homeostasis that gives insights into the aging of a stem cell compartment.

Many adult mammalian somatic tissues are maintained by resident stem and progenitor cell populations and show drastic age-dependent functional decline, which positively correlates with reduced cellular turnover (López-Otín et al., 2013). In mice, the generation of new olfactory bulb (OB) interneurons is sustained by subependymal zone (SEZ) adult neural stem cells (NSCs), whose output substantially decreases during aging (Blackmore et al., 2009; Bouab et al., 2011; Daynac et al., 2016; Mobley et al., 2013; Molofsky et al., 2006; Piccin et al., 2014). Declining neurogenesis has been associated with changes in local or systemic expression of (or responsiveness to) several factors (Chaker et al., 2015; Daynac et al., 2014; Enwere et al., 2004; Katsimpardi et al., 2014; Molofsky et al., 2006; Piccin et al.,

2014; Tropepe et al., 1997). Strikingly, it is still unclear if the proliferation of NSCs, and the migration, differentiation and survival of their progeny are affected by age in vivo. The abundance and proliferative activity of NSCs has been reported as decreasing with age (Enwere et al., 2004) or as being mostly unaffected (Daynac et al., 2014, 2016; Shook et al., 2012; Tropepe et al., 1997). Such conflicting views could stem from the different assays employed to evaluate NSC abundance and properties. These comprise *in vitro* assays of cellular behaviors (e.g. neurosphere-forming ability or growth as adherent cultures) known to be significantly affected by exposure to commonly employed mitogens (Costa et al., 2011; Hack et al., 2004; Petreanu and Alvarez-Buylla, 2002) and short-term *ex vivo* analyses of purified cell types (Codega et al., 2014). *In vivo* analyses without clonal lineage tracing (Petreanu and Alvarez-Buylla, 2002) allow for population dynamics snapshots, but are limited in the amount of information they can provide on the progeny of single stem cells.

To overcome these limitations, we recently employed *in vivo* clonal lineage tracing to qualitatively describe the predominant mode of neurogenic NSC activity in the SEZ of adult mice at the age of 2-3 months (from now on called 'young' mice) (Calzolari et al., 2015). Our observations support a model of adult OB neurogenesis whereby serial activation of dormant NSCs, followed by a phase of intense neuronal production, is often terminated by NSC exhaustion within a few weeks. While we posited that this process would gradually erode the dormant NSC pool, explaining the age-associated decline in neurogenic activity, it remained unclear if and to which extent changes in proliferation and differentiation during lineage progression play a role.

To tackle this issue, we performed an *in vivo* clonal lineage tracing analysis of adult murine OB neurogenesis at 12-14 months of age (from now on called 'old' mice). At this age neurogenesis is already markedly decreased compared to young adult mice, as reflected by the abundance of immature NSC progeny (Bouab et al., 2011; Daynac et al., 2014, 2016; Luo et al., 2006; Molofsky et al., 2006), and overall new OB neuron production (Bouab et al., 2011; Molofsky et al., 2006). We performed *in vivo* clonal lineage tracing using double hemizygous GLAST^{CreERT2}:Confetti transgenic mice (Calzolari et al., 2015; Mori and Tanaka, 2006; Ninkovic et al., 2007), and NSCs were clonally labeled with a single low dose of Tamoxifen (see Supplemental Experimental Procedures). We chose to analyze clones 21 or 56 days post-labeling (dpl; Figure 1A) based on our previous observations in young adult mice (analyzed at 7, 21, 35, and 56 dpl; Figure 1A), which had revealed a clear shift in clonal composition across this time window, from immature clones containing progenitors at earlier timepoints, to clones composed mostly of mature neurons at 56 dpi (Calzolari et al., 2015). We identified clonal components based on a combination of marker expression, localization and cell morphology (Figure 1B) in 46 clones from young mice (reported on in Calzolari et al., 2015) and 21 clones from old mice, in total counting 2336 single cells. To our surprise, clone size (Figure 1C) and spatial organization (Figure 1D) did not differ between young and old mice. Similarly to young animals, old clones showed rapid growth, comprising up to 110 cells already at 21 dpl (Figure 1A). The size, composition and distribution of clusters of TAPs/NBs in the SEZ and proximal rostral migratory stream (RMS) suggested multiple doublings as the basis for lineage amplification (Figure 1E), followed by coherent migration of related NBs (Figures 1F,G and S1A). These observations are similar to the ones in young animals obtained via *in vitro* (Costa et al., 2011) and *in vivo (Calzolari et al., 2015)* clonal analysis and population-level analyses (Ponti et al., 2013). Moreover, already at 21 dpl the overall spatial distribution of TAPs, NBs and neurons was compatible with multiple rounds of

NSC activation, resulting in the production of bouts of progeny then coherently undergoing maturation and migration (Figure 1G), similar to observations in young animals (Calzolari et al., 2015). Overall clonal maturation dynamics also resembled those observed in young mice; by 21 dpl most clones comprised either only progenitor cells (TAPs/NBs) or progenitors and neurons, with only a minority of clones (2/10) consisting of neurons only (Figure 1A). Eight weeks after labeling (56 dpl) the proportion of clones comprising only neurons had increased (4/11), albeit much less than in young animals, where 7 out of 12 clones consist of only neurons (Figure 1A). These clones were rarely found in association (i.e. in the same hemisphere) with a radial astrocyte (Figure 1H), suggestive of NSC exhaustion being the major mechanism of termination of NSC-derived OB neurogenesis, like in the young SEZ (Calzolari et al., 2015). Finally, the inter- and intra-clonal diversity and distribution of mature neurons in the OB also indicated consistency with the principles deduced from observations in young animals (Calzolari et al., 2015; Fuentealba et al., 2015; Merkle et al., 2013), with mostly subtype-restricted clonal neurogenic activity (Figure 1I,J; Figure S1B-F). These observations revealed that individual NSC clones active in the aged SEZ show no signs of grossly impaired neurogenic activity. This raised the possibility that subtle changes in clonal dynamics may underlie the known decline in overall neurogenic output from the aged SEZ. In order to quantify such features and compare competing hypotheses of clonal dynamics, we mathematically modelled adult neurogenesis at young and old ages with a stochastic population model (see Supplemental Experimental Procedures) using our clonal data and a limited set of published population-level data, as previously done for other systems (Chabab et al., 2016; Flossdorf et al., 2015; Yang et al., 2015).

Murine NSC heterogeneity (besides regionalization (Merkle et al., 2007, 2013)) is well appreciated molecularly and functionally (Codega et al., 2014; Dulken et al., 2017; Llorens-Bobadilla et al., 2015) and evidence exists for interconversion between actively proliferating and temporarily quiescent states (Basak et al., 2012; Costa et al., 2011; Giachino et al., 2014). Dormancy is a recognized feature of the majority of (young adult) NSCs (Shook et al., 2012; Urbán et al., 2016), possibly since late prenatal times (Falk et al., 2017; Fuentealba et al., 2015; Furutachi et al., 2015). We thus modeled the adult neurogenic lineage as comprising three NSC states (fully “dormant” (dS), “quiescent” (qS) and proliferating, “active” (aS) cells), TAPs, proliferating (NB I) and non-proliferating (NB II) neuroblasts and neurons (N) (see Figure 2A, S2A and Supplemental Experimental Procedures for details on model construction). By defining activation and inactivation, proliferation, migration and death rates as parameters for each state, we set up stochastic reaction rate equations that model clonal dynamics. For the three proliferating states (aS, TAP, NB, see Figure 2A), we each allow for four different division strategies: asymmetric (A), symmetric (S), constrained (C), where the proportion of symmetric and asymmetric divisions is regulated by a single parameter p_d, and unconstrained (U), where any combination of asymmetric division, self-renewal and symmetric differentiation probabilities is allowed, giving rise to an additional parameter (see Figure 2B and Supplemental Experimental Procedures for details). We here define an asymmetric division as a cell division followed by transition of only one daughter cell to the next stage in our model (Figure 2A) before it possibly divides again. Of note, the model does not differentiate whether this transition is coupled to the division, or if it happens some time after the cell has divided. The four different strategies result in $4^3 = 64$ different possible models with varying number of

parameters and complexity (Figure 2B). Unknown model parameters were estimated for each model separately by fitting means and variances of modeled TAPs, NBs, and Ns to means and variances of the measured clonal compositions (Figure S2B) using maximum likelihood estimation (Buchholz et al., 2013; Kazeroonian et al., 2016). The 64 different models were compared according to the Bayesian Information Criterion (BIC), a score that ranks models based on both their complexity and their ability to explain the observed data (Figure S2C). The ten best performing models (Figure 2C) indicate that changes in the division strategy of active NSCs are required to explain the observed clonal dynamics: While in young mice the best models require symmetric stem cell divisions (allowed by symmetric (S), constrained (C) and unconstrained (U) division strategies), asymmetric (A) stem cell divisions suffice to explain clonal measurements in old mice (Figure 2C) in the top seven models.

However, comparing the best-ranking models (see Figure 2D for cell fractions fitted with the best model for young and old mice) we do not find a single best model; instead, for the top ten models for clones at 2 and 14 months, differences in the BIC values below 4 are observed (Figures 2C and S2C), which are not considered decisive (Kass and Raftery, 1995). Therefore, we derived average models for young and old mice by weighting resulting parameter estimates with the posterior probability of their model (BIC weight, see Supplemental Experimental Procedures and Figure S2D) to yield robust model predictions. To evaluate the average model for young mice, we compared it to independent population-level data (Daynac et al., 2016; Shook et al., 2012) on the temporal evolution of cell type abundances during aging (Figure 2E). An adaptation of the average parameters from young to old mice (using Hill kinetics, see Supplemental Experimental Procedures and Figure S2F) leads to an age-dependent model that describes the decrease of TAPs and neuroblasts similarly well and allows for a prediction of cell numbers also for mice beyond 14 months.

Based on the weighted average proportion of symmetric self renewal, symmetric differentiation, and asymmetric division (Figure 2F), we find that asymmetric stem cell divisions are more prevalent in old compared to young mice (82,8±11,7% vs. 55,3±8,3% in young mice, mean±variance of averaged probabilities), while symmetric differentiation decreases from 36,6±4,1% in young mice to 14,6±8,9% in old mice. Our models also identify a high, age-independent percentage of symmetric self renewal of TAPs (27,0±1,4% in young, 24,4±1,5% in old mice), and rapid differentiation of neuroblasts, two properties that are consistent with the existing knowledge about these cell types (Calzolari et al., 2015; Costa et al., 2011; Ponti et al., 2013).

To investigate why the neuronal output diminishes during ageing, despite active stem cells dividing more often asymmetrically, we generated clonal genealogies from the estimated parameters (see Supplemental Experimental Procedures and Figure S2G). We simulated 1000 clones for young and old mice using the inferred weighted average parameters (see Figure 2G and S2E) and calculated genealogical metrics (Figure S2H) to compare clonal dynamics during aging. Interestingly, increased asymmetric NSC divisions change clonal dynamics in old mice (Figure 2H-J). Our model thus predicts an increase in asymmetric clonal dynamics resulting in the generation of more, but smaller and shorter-lived subclones in old mice. While enabling persistent neurogenesis, this produces a reduced neurogenic output at the population level. It is tempting to speculate that some of the inferred potentially “pro-neurogenic” changes in lineage transition parameters (e.g. increased aS asymmetric

division probability) may reflect the action of mechanisms at play to compensate for age-associated neurogenesis-depleting processes, such as the progressive activation and loss of dormant NSCs.

In conclusion, we have performed the first *in vivo* clonal analysis of neural stem cell behavior in aged adult mammals and mathematically modelled adult neurogenesis to define quantitative aspects of lineage transition in young and aged mice. Our model fits the observed data and unveils changes in a restricted set of key parameters. These parameters lead to relatively minor alterations in clonal dynamics, which however explain the observed stronger tendency of young animals to produce mature clones (Figure 1A) and are in agreement with drastic population-level age-related decline in adult OB neurogenesis.

ACKNOWLEDGEMENTS

We thank M. Goetz (LMU Munich and Helmholtz Zentrum München) for comments on the manuscript, A. Kazeroonian (TUM Munich) and C. Loos (Helmholtz Zentrum München) for computational support.

LB was supported by the German Research Foundation (DFG) within the Collaborative Research Centre 1243, Subproject A17. FC was supported in part by NEURON-ERANET (01EW1604) and DFG (CRC1080) grants to Dr. Benedikt Berninger (UMC Mainz) and by intramural funds to F.C.

AUTHOR CONTRIBUTIONS

FC generated data. LB and FC analyzed data. LB constructed model with FC. LB performed parameter inference and model simulations with support from MS and advice from JH and FT. FC and JN initiated the project with FT. JN and CM supervised the study. LB, FC, JN and CM wrote the paper.

SUPPLEMENTAL INFORMATION

Supplemental information on our experimental and computational strategy can be found in the SUPPLEMENTAL EXPERIMENTAL PROCEDURES. Code is available at https://github.com/QSCD/NeurogenesisAnalysis

REFERENCES

Basak, O., Giachino, C., Fiorini, E., Macdonald, H.R., and Taylor, V. (2012). Neurogenic subventricular zone stem/progenitor cells are Notch1-dependent in their active but not quiescent state. J. Neurosci. *32*, 5654–5666.

Blackmore, D.G., Golmohammadi, M.G., Large, B., Waters, M.J., and Rietze, R.L. (2009). Exercise Increases Neural Stem Cell Number in a Growth Hormone-Dependent Manner, Augmenting the Regenerative Response in Aged Mice. Stem Cells *27*, 2044–2052.

Bouab, M., Paliouras, G.N., Aumont, A., Forest-Bérard, K., and Fernandes, K.J.L. (2011). Aging of the subventricular zone neural stem cell niche: evidence for quiescence-associated changes between early and mid-adulthood. Neuroscience *173*, 135–149.

Buchholz, V.R., Flossdorf, M., Hensel, I., Kretschmer, L., Weissbrich, B., Gräf, P., Verschoor, A., Schiemann, M., Höfer, T., and Busch, D.H. (2013). Disparate individual fates compose robust CD8+ T cell immunity. Science *340*, 630–635.

Calzolari, F., Michel, J., Baumgart, E.V., Theis, F., Götz, M., and Ninkovic, J. (2015). Fast clonal expansion and limited neural stem cell self-renewal in the adult subependymal zone. Nat. Neurosci. *18*, 490–492.

Chabab, S., Lescroart, F., Rulands, S., Mathiah, N., Simons, B.D., and Blanpain, C. (2016). Uncovering the Number and Clonal Dynamics of Mesp1 Progenitors during Heart Morphogenesis. Cell Rep. *14*, 1–10.

Chaker, Z., Aïd, S., Berry, H., and Holzenberger, M. (2015). Suppression of IGF-I signals in neural stem cells enhances neurogenesis and olfactory function during aging. Aging Cell *14*, 847–856.

Codega, P., Silva-Vargas, V., Paul, A., Maldonado-Soto, A.R., Deleo, A.M., Pastrana, E., and Doetsch, F. (2014). Prospective identification and purification of quiescent adult neural stem cells from their in vivo niche. Neuron *82*, 545–559.

Costa, M.R., Ortega, F., Brill, M.S., Beckervordersandforth, R., Petrone, C., Schroeder, T., Götz, M., and Berninger, B. (2011). Continuous live imaging of adult neural stem cell division and lineage progression in vitro. Development *138*, 1057–1068.

Daynac, M., Pineda, J.R., Chicheportiche, A., Gauthier, L.R., Morizur, L., Boussin, F.D., and Mouthon, M.-A. (2014). TGFβ lengthens the G1 phase of stem cells in aged mouse brain. Stem Cells *32*, 3257–3265.

Daynac, M., Morizur, L., Chicheportiche, A., Mouthon, M.-A., and Boussin, F.D. (2016). Age-related neurogenesis decline in the subventricular zone is associated with specific cell cycle regulation changes in activated neural stem cells. Sci. Rep. *6*, 21505.

Dulken, B.W., Leeman, D.S., Boutet, S.C., Hebestreit, K., and Brunet, A. (2017). Single-Cell Transcriptomic Analysis Defines Heterogeneity and Transcriptional Dynamics in the Adult Neural Stem Cell Lineage. Cell Rep. *18*, 777–790.

Enwere, E., Shingo, T., Gregg, C., Fujikawa, H., Ohta, S., and Weiss, S. (2004). Aging results in reduced epidermal growth factor receptor signaling, diminished olfactory

neurogenesis, and deficits in fine olfactory discrimination. J. Neurosci. *24*, 8354–8365.

Falk, S., Bugeon, S., Ninkovic, J., Pilz, G.-A., Postiglione, M.P., Cremer, H., Knoblich, J.A., and Götz, M. (2017). Time-Specific Effects of Spindle Positioning on Embryonic Progenitor Pool Composition and Adult Neural Stem Cell Seeding. Neuron *93*, 777–791.e3.

Flossdorf, M., Rössler, J., Buchholz, V.R., Busch, D.H., and Höfer, T. (2015). CD8(+) T cell diversification by asymmetric cell division. Nat. Immunol. *16*, 891–893.

Fuentealba, L.C., Rompani, S.B., Parraguez, J.I., Obernier, K., Romero, R., Cepko, C.L., and Alvarez-Buylla, A. (2015). Embryonic Origin of Postnatal Neural Stem Cells. Cell *161*, 1644–1655.

Furutachi, S., Miya, H., Watanabe, T., Kawai, H., Yamasaki, N., Harada, Y., Imayoshi, I., Nelson, M., Nakayama, K.I., Hirabayashi, Y., et al. (2015). Slowly dividing neural progenitors are an embryonic origin of adult neural stem cells. Nat. Neurosci. *18*, 657–665.

Giachino, C., Basak, O., Lugert, S., Knuckles, P., Obernier, K., Fiorelli, R., Frank, S., Raineteau, O., Alvarez-Buylla, A., and Taylor, V. (2014). Molecular diversity subdivides the adult forebrain neural stem cell population. Stem Cells *32*, 70–84.

Hack, M.A., Sugimori, M., Lundberg, C., Nakafuku, M., and Götz, M. (2004). Regionalization and fate specification in neurospheres: the role of Olig2 and Pax6. Mol. Cell. Neurosci. *25*, 664–678.

Kass, R.E., and Raftery, A.E. (1995). Bayes Factors. J. Am. Stat. Assoc. *90*, 773.

Katsimpardi, L., Litterman, N.K., Schein, P.A., Miller, C.M., Loffredo, F.S., Wojtkiewicz, G.R., Chen, J.W., Lee, R.T., Wagers, A.J., and Rubin, L.L. (2014). Vascular and neurogenic rejuvenation of the aging mouse brain by young systemic factors. Science *344*, 630–634.

Kazeroonian, A., Fröhlich, F., Raue, A., Theis, F.J., and Hasenauer, J. (2016). CERENA: ChEmical REaction Network Analyzer--A Toolbox for the Simulation and Analysis of Stochastic Chemical Kinetics. PLoS One *11*, e0146732.

Llorens-Bobadilla, E., Zhao, S., Baser, A., Saiz-Castro, G., Zwadlo, K., and Martin-Villalba, A. (2015). Single-Cell Transcriptomics Reveals a Population of Dormant Neural Stem Cells that Become Activated upon Brain Injury. Cell Stem Cell *17*, 329–340.

López-Otín, C., Blasco, M.A., Partridge, L., Serrano, M., and Kroemer, G. (2013). The hallmarks of aging. Cell *153*, 1194–1217.

Luo, J., Daniels, S.B., Lennington, J.B., Notti, R.Q., and Conover, J.C. (2006). The aging neurogenic subventricular zone. Aging Cell *5*, 139–152.

Merkle, F.T., Mirzadeh, Z., and Alvarez-Buylla, A. (2007). Mosaic organization of neural stem cells in the adult brain. Science *317*, 381–384.

Merkle, F.T., Fuentealba, L.C., Sanders, T.A., Magno, L., Kessaris, N., and Alvarez-Buylla, A. (2013). Adult neural stem cells in distinct microdomains generate previously unknown interneuron types. Nat. Neurosci. *17*, 207–214.

Mobley, A.S., Bryant, A.K., Richard, M.B., Brann, J.H., Firestein, S.J., and Greer, C.A. (2013). Age-dependent regional changes in the rostral migratory stream. Neurobiol. Aging

34, 1873–1881.

Molofsky, A.V., Slutsky, S.G., Joseph, N.M., He, S., Pardal, R., Krishnamurthy, J., Sharpless, N.E., and Morrison, S.J. (2006). Increasing p16INK4a expression decreases forebrain progenitors and neurogenesis during ageing. Nature *443*, 448–452.

Mori, T., and Tanaka, T. (2006). Effect of transition metal doping and carbon doping on thermoelectric properties of YB66 single crystals. J. Solid State Chem. *179*, 2889–2894.

Ninkovic, J., Mori, T., and Götz, M. (2007). Distinct modes of neuron addition in adult mouse neurogenesis. J. Neurosci. *27*, 10906–10911.

Petreanu, L., and Alvarez-Buylla, A. (2002). Maturation and death of adult-born olfactory bulb granule neurons: role of olfaction. J. Neurosci. *22*, 6106–6113.

Piccin, D., Tufford, A., and Morshead, C.M. (2014). Neural stem and progenitor cells in the aged subependyma are activated by the young niche. Neurobiol. Aging *35*, 1669–1679.

Ponti, G., Obernier, K., Guinto, C., Jose, L., Bonfanti, L., and Alvarez-Buylla, A. (2013). Cell cycle and lineage progression of neural progenitors in the ventricular-subventricular zones of adult mice. Proc. Natl. Acad. Sci. U. S. A. *110*, E1045–E1054.

Shook, B.A., Manz, D.H., Peters, J.J., Kang, S., and Conover, J.C. (2012). Spatiotemporal changes to the subventricular zone stem cell pool through aging. J. Neurosci. *32*, 6947–6956.

Tropepe, V., Craig, C.G., Morshead, C.M., and van der Kooy, D. (1997). Transforming growth factor-alpha null and senescent mice show decreased neural progenitor cell proliferation in the forebrain subependyma. J. Neurosci. *17*, 7850–7859.

Urbán, N., van den Berg, D.L.C., Forget, A., Andersen, J., Demmers, J.A.A., Hunt, C., Ayrault, O., and Guillemot, F. (2016). Return to quiescence of mouse neural stem cells by degradation of a proactivation protein. Science *353*, 292–295.

Yang, J., Plikus, M.V., and Komarova, N.L. (2015). The Role of Symmetric Stem Cell Divisions in Tissue Homeostasis. PLoS Comput. Biol. *11*, e1004629.

FIGURE CAPTIONS

Figure 1: In vivo clonal measurements of neural stem cells (NSCs) in the subependymal zone (SEZ) of young and old mice.

(A) Experimental design. The clonal progeny of a single labeled NSC is observed at one of four different time points (7, 21, 35 and 56 days post labeling) in young (white) and old (grey) mice. The progeny is classified into four cell types: NSC, Transit-amplifying progenitor (TAP), neuroblast (NB) and neuron (N). Pie charts detail the number and composition of clones observed at each time point. Size of pie charts reflect the clone size.

(B) Examples of cells at distinct stages of neurogenic lineage progression, as labelled in Glast^{CreERt2}-Confetti mice. Markers were used to positively identify cell states via GFAP (NSCs) and Dcx (NBs) expression. TAPs and Neurons were defined by a combination of lack of marker expression, localization and morphology. The proliferation marker Ki67 is shown to confirm the TAP identity of SEZ-localized Dcx-negative cells, but was not regularly used to identify cells. Dashed line highlights the LV border. Scale bars 20 µm.

(C) Average clone sizes at 21 and 56 days post labeling (dpl), for young and old mice. Data for young mice represent re-plotting of data from Calzolari et al. 2015. We show mean +/- S.E.M. (n=14,12 in young and n=12,11 in old mice respectively).

(D) Clonal average percentage of SEZ-encompassing sagittal sections comprising TAPs or NBs, revealing broader distribution for NBs than TAPs, a feature not affected by age. Data for young mice represent re-plotting of data from Calzolari et al. 2015. Error bars represent S.E.M.

(E) Average size of cell clusters of the indicated compositions, as found in the SEZ/Proximal RMS of aged mice. Error bars represent S.E.M.

(F) Example of subclonal expansion, showing clone components (Confetti reporter, green) distributed across three consecutive SEZ sections in a 1yo brain. Insets to the right focus on the most posterolateral section, where a single GFAP-positive cell is surrounded by clonally related cells (max-intensity projection of a reduced number of optical sections, to better highlight Confetti/GFAP colocalization). Yellow arrowheads point to GFAP signal in the soma and radial process. Dashed curves indicate SEZ borders, dashed box highlights the inset. LV, lateral ventricle. Scale bars 20 µm.

(G) Five exemplary clones (old) showing numbers of cells (y axes) per cell stage (color code) along the SEZ-to-OB axis, based on binning as indicated in the scheme above the panel, depicting a partial sagittal mouse brain section. RMS is subdivided in proximal (Prox), Descending/horizontal limbs (D/H) and RMS-OB (OB). Ocra OB refers to OB locations external to the RMS-OB.

(H) Percentage of clones, either comprising both progenitors and neurons (T/B/N) or only neurons (N), for which a radial astrocyte sharing the clone´s Confetti label could be found in the ipsilateral SEZ.

(I) Percentage of clones comprising the indicated OB neuronal subtypes, for both young and old mice. Data for young mice are from Calzolari et al. 2015.

(J) Normalized position of all neurons found in old mice, subdivided by clone, with number of neurons per clone indicated above the graph.

Figure 2: A population model fits the clonal data and predicts increased asymmetric stem cell divisions in old mice.

(A) Adult neurogenesis model: The pool of dormant stem cells (dS) is depleted over time. Cells can then be activated and inactivated by switching between the quiescent (qS) and active (aS) state. aS, Transit amplifying progenitors (TAPS) and neuroblasts of type I (NB I) divide. Neuroblasts of type II (NB II) no longer divide and migrate along the SEZ to eventually become neurons (N) that are depleted via cell death.

(B) Division strategies for dividing cell types: Asymmetric divisions (A) give rise to a daughter cell of the same type and a daughter cell of the subse- quent type, symmetric divisions (S) produce two daughters of the same cell type, constrained divisions (C) assume independent differentiation between sisters, while the unconstrained division (U) is the most flexible strategy. The number of model parameters increases from left to right with equal model complexity for strategies S and C.

(C) 64 different models are fitted separately to data from young and old mice and compared via the Bayesian information criterion (BIC). Columns belong to cell types shown in A. Asymmetric stem cell divisions are prevalent in the best 10 models for old mice.

(D) Mean cell fractions of best models (solid lines) vs. observed cell fractions (small grey dots) and their mean (large black dots) for TAPs, neuroblasts, and neurons. Model stochasticity is calculated from SSA simulations (gray shaded area, ±2 s.d. errors).

(E) Predicted cell numbers of age-dependent and age-independent weighted average models (solid and dashed lines) fit to population data from Daynac et al. (mean±2s.d., n>=4 per time point). Data points reflect number of cells per brain hemisphere. Initial conditions are set to earliest observed measurement of the respective cell type. Models include halfway migration of neuroblasts in order to be consistent with the population study data. Data points reflect number of cells per brain hemisphere.

(F) Division probabilities calculated from all 64 models as a weighted average according to their BIC weights for young (white) and old (shaded) mice shows strong TAP self renewal (top), rapid NB differentiation (middle), and increased asymmetric stem cell divisions in old mice (bottom). Error bars indicate ± standard error of the weighted mean ($S.E.M._w$).

(G) n=4 trees simulated according to average models and parameter distributions introduced in (G) for young (left) and old (right), respectively.

(H) Absolute frequency of subclones and inactive branches (resulting from aS return to quiescence without any division) per clone in young and old. Numbers were estimated from n=1000 simulated lineage trees according to the average young and old model for 100 days.

(I) Mean subclonal branch length and

(J) Subclonal lifespan from 1000 simulated lineage trees from the average young and old model. Medians are shown as a black line.

Figure S1:

(A) Examples of NB/TAP distribution, showing the number and identity of cells, belonging to two distinct clones, found in each sagittal brain slice. Slices are numbered consistently across brains from the medial-most slice. Outlines above the graph refer to the indicated slices and provide an overview of the position and local extent of the SEZ, highlighted in yellow.

(B) Examples of the variety of OB neuronal subtypes observed. Scale bar 20µm.

(C) Overall distribution of all OB neurons observed in old mice; y-axis reports the percentage of neurons found within a given normalized distance bin (shown on the x-axis; 0=RMS-OB, 1=GCL/IPL boundary). Deep and superficial granule neuron domains are clearly distinguishable as distinct distributions.

(D) Average intraclonal abundance of each neuronal subtype, in young and old mice.

(E) Average intraclonal abundance of each neuronal subtype, when prevalent (i.e. when ≥50% of all neurons in the clone), in young and old mice.

(F) Percentage of clones being enriched (as defined in E) for the indicated neuronal subtypes, in young and old mice. Data for young mice are re-plot from Calzolari et al. 2015.

Figure S2:

(A) ODE stem cell compartment model (top), fitted to data from Shook et al. (number of active stem cell and total number of stem cells) & Daynac et al. (number of active stem cells and quiescent stem cells), shown as mean ±2 s.d. (n>4 per time point) (middle). Data points reflect number of neural stem cells per brain hemisphere. Rate estimates in table were used to constrain model of neurogenesis.

(B) Rank 1 young and old models (solid lines) fit to experimental 1st and 2nd order moments (large dots). Standard deviation of experimental moments were calculated via bootstrapping from single clonal observations (small dots in upper row) and shown as ±2std error band (grey shaded area).

(C) BIC differences for all 64 models to the rank 1 model for young (solid line) and old (dashed line) mice.

(D) Estimated posterior model probability (BIC weights) for young (solid line) and old (dashed line) mice indicate that the top ten models dominate.

(E) Hill function fits to model a smooth age-dependent change in weighted average parameters that differ between young and old.

(F) Histograms for young (white) and old (grey) showing resulting parameters for all 64 models. Horizontal lines show weighted average parameters for young (solid) and old (dashed).

(G) Biologically plausible distributions for (in)activation, division, migration and death times, which are assumed for tree simulations. Horizontal lines show mean of distribution (weighted average rates).

(H) Definition of genealogical metrics.

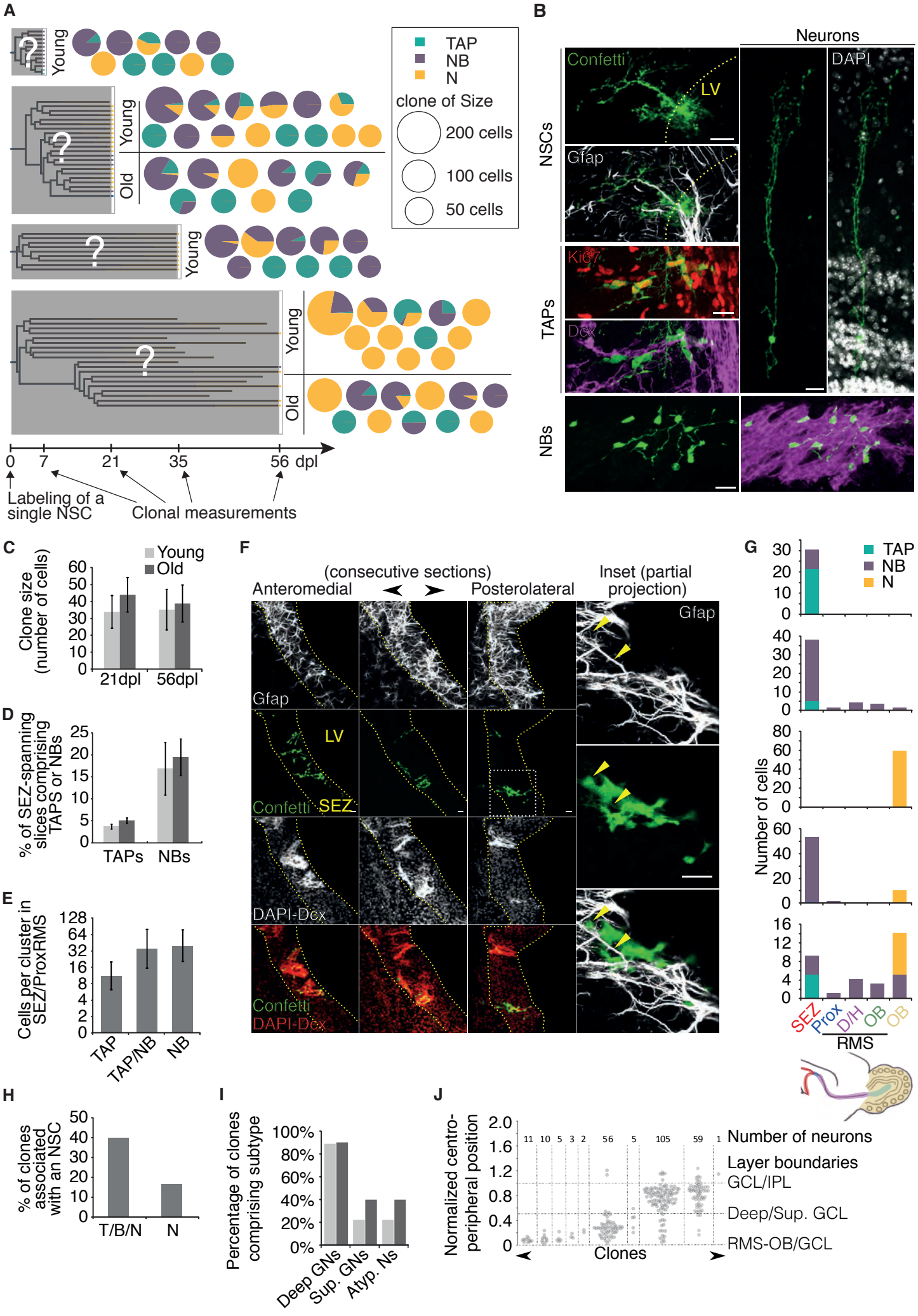

Figure 1: In vivo clonal measurements of neural stem cells (NSCs) in the subependymal zone (SEZ) of young and old mice.

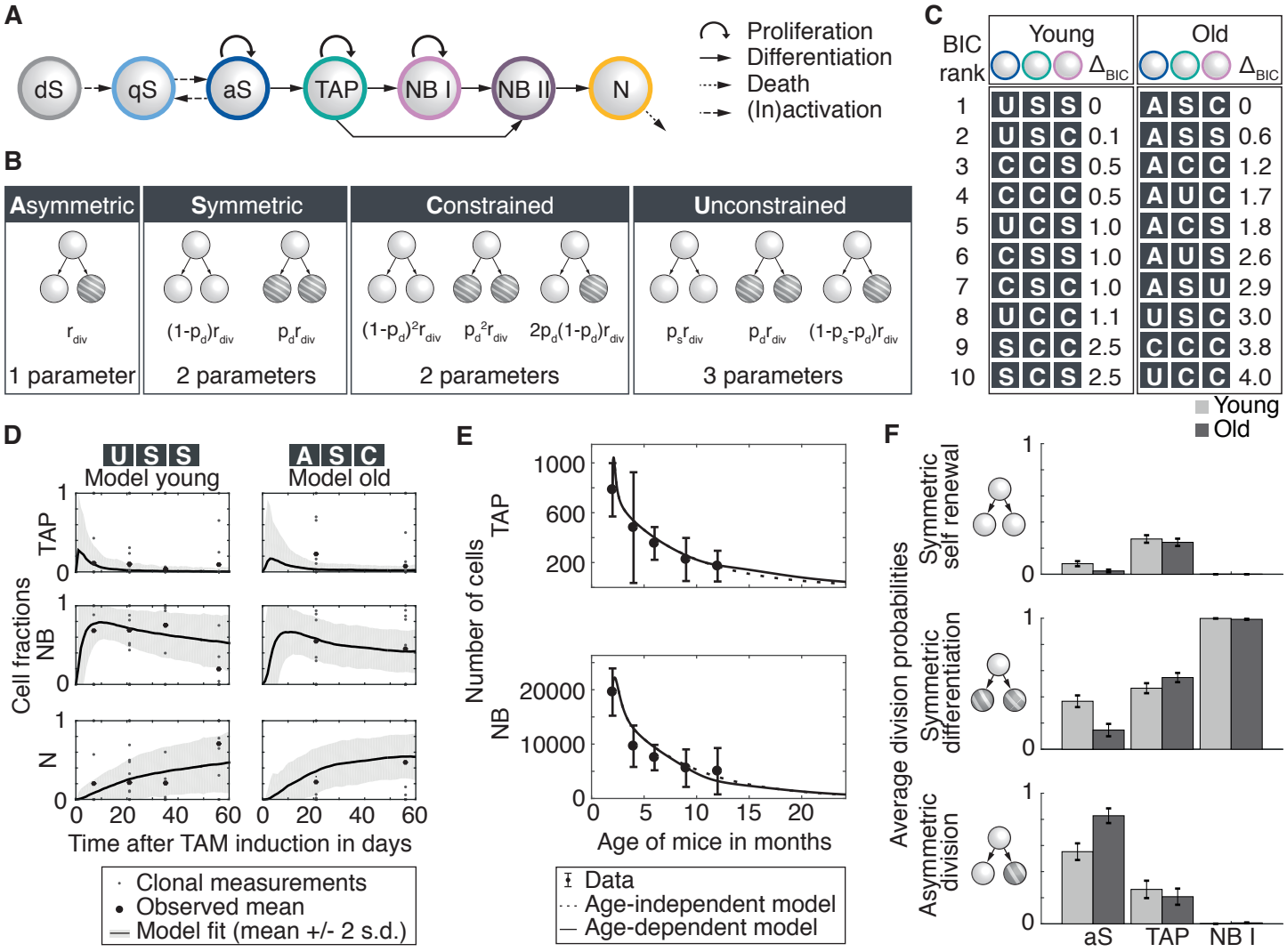

Figure 2: A population model fits the clonal data and predicts increased asymmetric stem cell divisions in old mice.

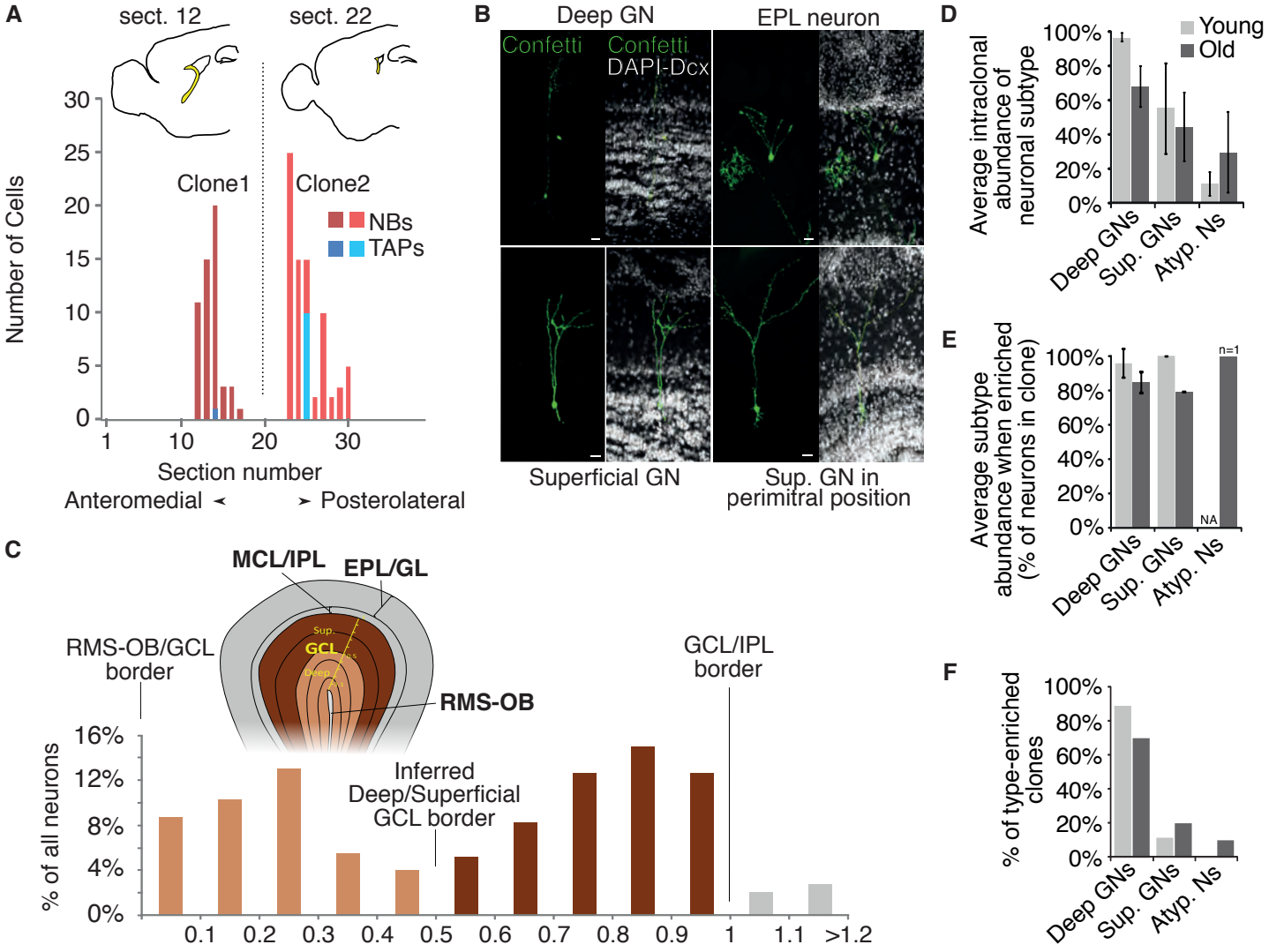

Figure S1

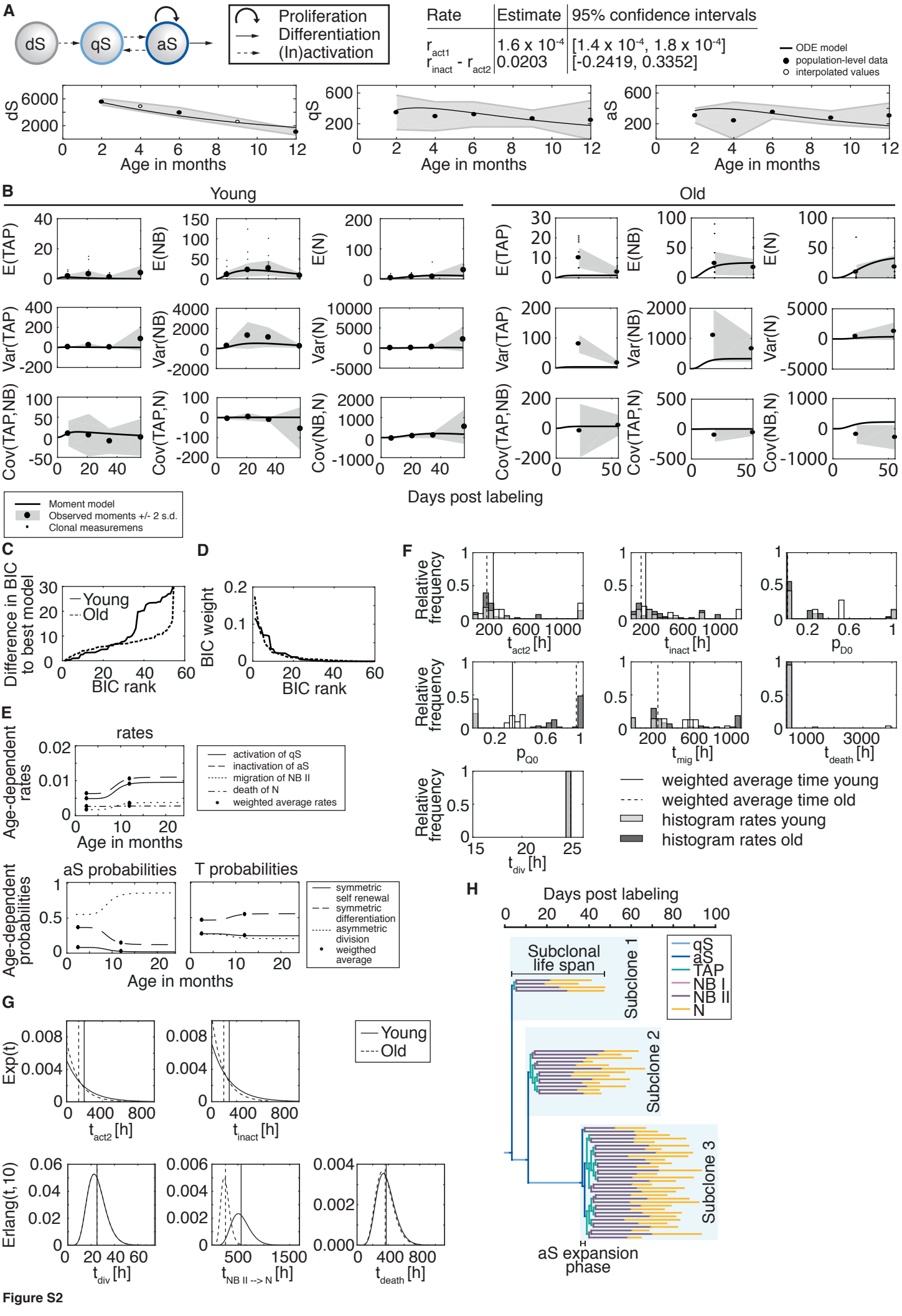

Figure S2